

Reference Code: hess-2018-393

Title: Spatially dependent flood probabilities to support the design of civil infrastructure systems

Corresponding Author: Phuong Dong Le (The University of Adelaide)

Contributing Authors: Michael Leonard and Seth Westra

Response to the Reviewer

The authors have significantly modified and improved the manuscript, taking into account my comments. In particular the model is now much more clearly presented for HESS readers.

Response: Thank you for your comments. We respond in detail below (your comments in italic font and our responses in normal font).

Major comment #1:

My only significant comment regards the Authors' response to my previous Minor comment #14. Indeed using an inverted max-stable process rather than a Gaussian process -the two of them are Alcomplicates much the theory, model estimation and simulation. I know that max-stable processes are theoretically founded for AD models (see Schlather 2002) but what about inverted max-stable processes for AI models? I might be wrong but I don't think there is any theory saying that inverted max-stable process are well-founded for AI models. Given that this article will be mainly read by non-statisticians, I do wonder what is gained by using the inverted max-stable process rather than a Gaussian process, which is much easier to handle. I understand that model comparison is not the goal of the paper but could the authors please better justify their choice for the inverted max-stable model? Otherwise it sound like using a sledgehammer to crack a nut.

Response:

This study uses an asymptotically independent model, of which multiple types are valid including the Gaussian copula (Davison et al., 2012) and inverted max-stable processes (Wadsworth and Tawn, 2012). The inverted max-stable model was ultimately selected in this study to provide consistency with our earlier paper (i.e. "Dependence properties of spatial rainfall extremes and areal reduction factors", in Journal of Hydrology), in which it was demonstrated to preserve the spatial properties of extreme rainfall in an Australian context, including the property of asymptotic independence. Thibaud et al (2013) compared the inverted max-stable model with a Gaussian copula in a case study in Switzerland, and identified that the inverted max-stable model was appropriate.

We note in the manuscript that both models are plausible for asymptotically independent extremes, but in the context of the contribution of this paper (which is an application of joint extremes in an engineering design context), we feel that the inverted-max stable model is well-supported by the data and suitable to illustrate the main concepts.¹

Minor comment #1:

– L 69-69: *"This is likely to be because"* → *this is likely because*

Response: We have fixed this.

¹ Line 239: "This study uses an asymptotically independent model, of which multiple types are valid including the Gaussian copula ([Davison et al., 2012](#)) and inverted max-stable processes ([Wadsworth and Tawn, 2012](#)). The inverted max-stable model was ultimately selected in this study to provide consistency earlier research ([Le et al., 2018a](#)), in which it was demonstrated to preserve the spatial properties of extreme rainfall in an Australian context, including the property of asymptotic independence. [Thibaud et al. \(2013\)](#) also compared the inverted max-stable model with a Gaussian copula in a case study in Switzerland, and identified that the inverted max-stable model was appropriate."

Line 500: "Although this study focused on the inverted max-stable model to simulate the extreme rainfall process, other methods such as the Gaussian copula may also be appropriate and should be considered in future applications."

Minor comment #2:

– L 102: *a more applied work on max-stable process for extreme rainfall is: Blanchet, J. & Creutin, J.-D. (2017), 'Co-Occurrence of Extreme Daily Rainfall in the French Mediterranean Region', Water Resources Research 53(11), 9330–9349.*

Response: We have included this paper into the literature in the updated manuscript.² Thanks!

Minor comment #3:

– L 228: *“fit to observed rainfall” → above some large threshold, I guess*

Response: We have fixed this.

Minor comment #4:

– L 130: *“on average only once on average”*

Response: We have changed this. Thank you!

Minor comment #5:

– *Figure 4: actually, don't you only fit the marginal model (GPD) above the threshold?*

Response: Thanks. We have clarified this.

Minor comment #6:

– L 313-314 and 316-317: *isn't this a repetition?*

Response: Thanks for pointing it out. We have removed the latter one.

Minor comment #7:

– L 376: *“which the dependence model” → syntax issue*

Response: We have fixed this sentence. Thanks!

Minor comment #8:

– L 431-437: *“the covariance element ... 9 hr” → isn't it possible to make one sentence from these two (for two durations D1 and D2 in general)?*

Response: We think that the current text is OK because the two sentences put emphasis on how to calculate the covariance element for the same duration and for different durations. So, we have decided to keep these sentences.

² Line 90: “Max-stable process has also been used to represent the co-occurrence of extreme daily rainfall in the French Mediterranean region ([Blanchet and Creutin, 2017](#))”

Minor comment #9:

– L 717: “*all of events*” → *all the events*

Response: We have fixed this.

Spatially dependent flood probabilities to support the design of civil infrastructure systems

Phuong Dong Le^{1,2}, Michael Leonard¹, Seth Westra¹

¹*School of Civil, Environmental and Mining Engineering, University of Adelaide, Adelaide, South Australia, Australia*

²*Thuyloi University, [175 Tay Son, Dong Da, Hanoi, Vietnam](#)*

Email: lephuongdong_tb@tlu.edu.vn

Keywords: areal reduction factor, asymptotic independence, conditional probability, duration dependence, extreme rainfall, flood probability, inverted max-stable process, joint probability, spatially dependent Intensity-Duration-Frequency

Abstract

Conventional flood risk methods typically focus on estimation at a single location, which can be inadequate for civil infrastructure systems such as road or railway infrastructure. This is because rainfall extremes are spatially dependent, so that to understand overall system risk it is necessary to assess the interconnected elements of the system jointly. For example, when designing evacuation routes it is necessary to understand the risk of one part of the system failing given that another region is flooded or exceeds the level at which evacuation becomes necessary. Similarly, failure of any single part of a road section (e.g., a flooded river crossing) may lead to the wider system's failure (i.e. the entire road becomes inoperable). This study demonstrates a spatially dependent Intensity-Duration-Frequency framework that can be used to estimate flood risk across multiple catchments, accounting for dependence both in space and across different critical storm durations. The framework is demonstrated via a case study of a highway upgrade, comprising five river crossings. The results show substantial differences in conditional and unconditional design flow estimates, highlighting the importance of taking an integrated approach. There is also a reduction in the estimated failure probability of the overall system compared with the case where each river crossing is treated independently. The results demonstrate the potential uses of spatially dependent Intensity-Duration-Frequency methods and suggest the need for more conservative design estimates to take into account conditional risks.

29 **1. Introduction**

30 Methods for quantifying the flood risk of civil infrastructure systems such as road and rail networks
31 require considerably more information compared to traditional methods that focus on flood risk at a
32 point. For example, the design of evacuation routes requires the quantification of the risk that one part
33 of the system will fail at the same time that another region is flooded or exceeds the level at which
34 evacuation becomes necessary. Similarly, a railway route may become impassable if any of a number
35 of bridges are submerged, such that the ‘failure probability’ of that route becomes some aggregation of
36 the failure probabilities of each individual section. Successful estimation of flood risk in these systems
37 therefore requires recognition both of the networked nature of the civil infrastructure system across a
38 spatial domain, as well as the spatial and temporal structure of flood-producing mechanisms (e.g. storms
39 and extreme rainfall) that can lead to system failure (e.g., [Leonard et al. \(2014\)](#), [Seneviratne et al.
40 \(2012\)](#), [Zscheischler et al. \(2018\)](#)).

41 One way to estimate such flood probabilities is to directly use information contained in historical
42 streamflow data. For example, annual maximum streamflow at two locations might be assumed to
43 follow a bivariate generalized extreme value distribution ([Favre et al., 2004](#); [Wang, 2001](#); [Wang et al.,
44 2009](#)), which can then be used to estimate both conditional probabilities (e.g. the probability that one
45 river is flooded given that the other river level exceeds a specified threshold) and joint probabilities
46 (e.g. the probability that one or both rivers are flooded). Several frameworks have been demonstrated
47 based directly on streamflow observations, including functional regression ([Requena et al., 2018](#)),
48 multisite copulas ([Renard and Lang, 2007](#)), and spatial copulas ([Durocher et al., 2016](#)). However, in
49 many instances continuous streamflow data are unavailable or insufficient at the locations of interest,
50 or the catchment conditions have changed such that historical streamflow records as unrepresentative
51 of likely future risk. For these situations, rainfall-based methods are often more appropriate.

52 There are two primary classes of rainfall-based methods to estimate flood probability. The first uses
53 continuous rainfall data (either historical or generated) to compute continuous streamflow data using a
54 rainfall-runoff model ([Boughton and Droop, 2003](#); [Cameron et al., 1999](#); [He et al., 2011](#); [Hegnauer et
55 al., 2014](#); [Pathiraja et al., 2012](#)), with flood risk then estimated based on the simulated streamflow time

56 series. This method is computationally intensive and given the challenge of reproducing a wide variety
57 of statistics across many scales, can have difficulties in modelling the dependence of extremes. Most
58 spatial rainfall models operate at the daily timescale ([Bárdossy and Pegram, 2009](#); [Baxevani and](#)
59 [Lennartsson, 2015](#); [Bennett et al., 2016b](#); [Hegnauer et al., 2014](#); [Kleiber et al., 2012](#); [Rasmussen, 2013](#)),
60 whereas many catchments respond at sub-daily timescales. This is likely ~~to be~~ because the capacity of
61 space-time rainfall models to simulate the statistics of sub-daily rainfall remains a challenging research
62 problem ([Leonard et al., 2008](#)), although one approach is to exploit the relative abundance of data at
63 the daily scale, then apply a downscaling model to reach sub-daily scales ([Gupta and Tarboton, 2016](#)).
64 Continuous simulation is receiving ongoing attention and increasing application, yet there remain
65 limitations when applying these models in many practical contexts.

66 The second rainfall-based method proceeds by applying probability calculations on rainfall, to construct
67 ‘Intensity-Duration-Frequency’ (IDF) curves, which are then translated to a runoff event of equivalent
68 probability either via empirical models such as the rational method to estimate peak flow rate
69 ([Kuichling, 1889](#); [Mulvaney, 1851](#)), or via event-based rainfall-runoff models that are able to simulate
70 the full flood hydrograph ([Boyd et al., 1996](#); [Chow et al., 1988](#); [Laurenson and Mein, 1997](#)). Regional
71 frequency analysis is one type of method to estimate IDF values, where the precision of at-site estimates
72 is improved by pooling data from sites in the surrounding region ([Hosking and Wallis, 1997](#)). These
73 methods can be combined with spatial interpolation methods to estimate parameters for any ungauged
74 location of interest ([Carreau et al., 2013](#)). To determine an effective mean depth of rainfall over a
75 catchment with the same exceedance probability as at a gauge location, the pointwise estimate of
76 extreme rainfall is multiplied by an areal reduction factor (ARF) ([Ball et al., 2016](#)). However, such
77 methods do not account for information on the spatial dependence of extreme rainfall—whether for a
78 single storm duration, or for the more complex case of different durations across a region ([Bernard,](#)
79 [1932](#); [Koutsoyiannis et al., 1998](#)). The underlying independence assumption prevents these approaches
80 from being applied to estimate conditional or joint flood risk at multiple points in a catchment or across
81 several catchments, as would be required for a civil infrastructure system.

82 Although multivariate approaches can be tailored to estimate conditional and joint probabilities of
83 extreme rainfall for specific situations (e.g., [Kao and Govindaraju \(2008\)](#), [Wang et al. \(2010\)](#), [Zhang
84 and Singh \(2007\)](#)), the development of a unified methodology that integrates with existing IDF-based
85 flood estimation approaches remains elusive. This is particularly challenging given that it is not only
86 necessary to account for dependence of rainfall across space, but also to account for dependence across
87 storm burst durations, as different parts of the system may be vulnerable to different critical duration
88 storm events. To this end, max-stable process theory has been demonstrated to represent storm-level
89 dependence ([de Haan, 1984](#); [Schlather, 2002](#)) and used to calculate conditional probabilities for a spatial
90 domain ([Padoan et al., 2010](#)). [Max-stable process has also been used to represent the co-occurrence of
91 extreme daily rainfall in the French Mediterranean region \(Blanchet and Creutin, 2017\)](#). Copulas
92 including the extremal-t copula ([Demarta and McNeil, 2005](#)), and the Husler-Reiss copula ([Hüsler and
93 Reiss, 1989](#)) have also been used to model rainfall dependence.

94 This study applies a max-stable approach with an emphasis on practical flood estimation problems. To
95 this end, any proposed approach needs to account for:

- 96 1. The spatial dependence of rainfall ‘events’ both for single durations, and also across multiple
97 different durations. This was addressed by [Le et al. \(2018b\)](#), who linked a max-stable model
98 with the duration-dependent model of [Koutsoyiannis et al. \(1998\)](#), to create a model that could
99 be used to reflect dependencies between nearby catchments of different sizes.
- 100 2. The asymptotic properties of spatial dependence as the events become increasingly extreme,
101 given the focus of many flood risk estimation methods on rare flood events. Recent evidence is
102 emerging that rainfall has an asymptotically independent characteristic ([Le et al., 2018a](#);
103 [Thibaud et al., 2013](#)), which means that the level of the rainfall’s dependence reduces with an
104 increasing return period ([Wadsworth and Tawn, 2012](#)). The requirement of asymptotic
105 independence indicates that inverted max-stable models are preferable over max-stable models.

106 This study adapts the methods developed by [Le et al. \(2018b\)](#) to inverted max-stable models to derive
107 spatially-dependent IDF estimates and ARFs as the basis for transforming rainfall into flood flows. The
108 approach is demonstrated on a highway system spanning 20 km with five separate river crossings.

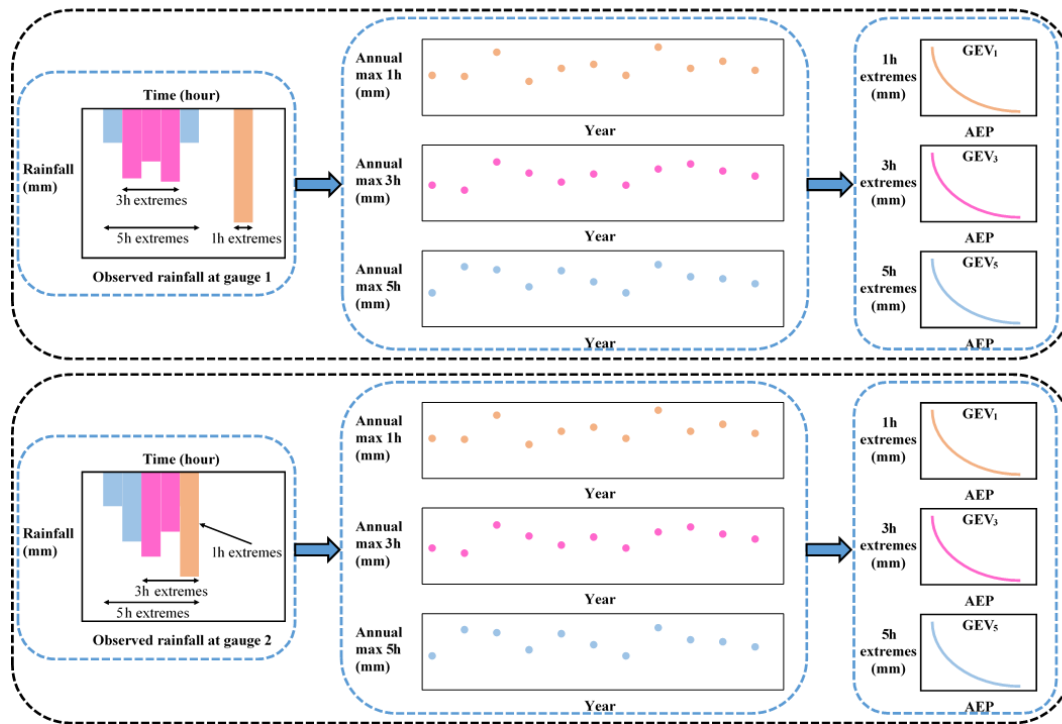
109 The case study is designed to address two related questions: (i) “What flood flow needs to be used to
110 design a bridge that will fail on average only once on average every M times given that a neighbouring
111 catchment is flooded?”; and (ii) “What is the probability that the overall system fails given that each
112 bridge is designed to a specific exceedance probability event (e.g., the 1% annual exceedance
113 probability event)?” The method for resolving these questions represents a new approach to estimate
114 flood risk for engineering design, by focusing attention on the risk of the entire system, rather than the
115 risk of individual system elements in isolation.

116 In the remainder of the paper, Section 2 emphasises the need for spatially dependent IDF estimates in
117 flood risk design, followed by Section 3 which outlines the case study and data used. Section 4 explains
118 the implementation of the framework, including a method for analysing the spatial dependence of
119 extreme rainfall across different durations. Results on the behaviour of floods due to the spatial and
120 duration dependence of rainfall extremes, are provided in Section 5. Conclusions and discussion follow
121 in Section 6.

122 **2. The need for spatially dependent IDF estimates in flood risk estimation**

123 The main limitation of conventional methods of flood risk estimation is that they isolate bursts of
124 rainfall and break the dependence structure of extreme rainfall. Figure 1 demonstrates a traditional
125 process of estimating at-site extreme rainfall for two locations (gauge 1, gauge 2) and three durations
126 (1, 3, and 5 hr) ([Stedinger et al., 1993](#)). The process first involves extracting the extreme burst of rainfall
127 for each site, duration and year from the continuous rainfall data, and then fitting a probability
128 distribution (such as the Generalised Extreme Value (GEV) distribution) to the extracted data. Figure 1
129 demonstrates that, through the process of converting the continuous rainfall data to a series of discrete
130 rainfall ‘bursts’, this process breaks the dependence both with respect to duration and space. Firstly, the
131 duration dependence is broken by extracting each duration separately, whereas for the hypothetical
132 storm in Fig. 1 it is clear that the annual maxima from some of the extreme bursts come from the same
133 storm. Secondly, the spatial dependence is broken because each site is analysed independently. Again,
134 for the hypothetical storm of Fig. 1 it can be seen that the 5 hr storm has occurred at the same time
135 across the two catchments, and this information is lost in the subsequent probability distribution curves.

136 Lastly, there is cross-dependence in space and duration. For example, the 1 hr extreme from gauge 2
 137 occurs at the same time as the 5 hr extreme from gauge 1. This may be relevant if there are two
 138 catchments with times of concentration matching 1 hr and 5 hr respectively, which can arise where
 139 catchments are neighbouring or nested.

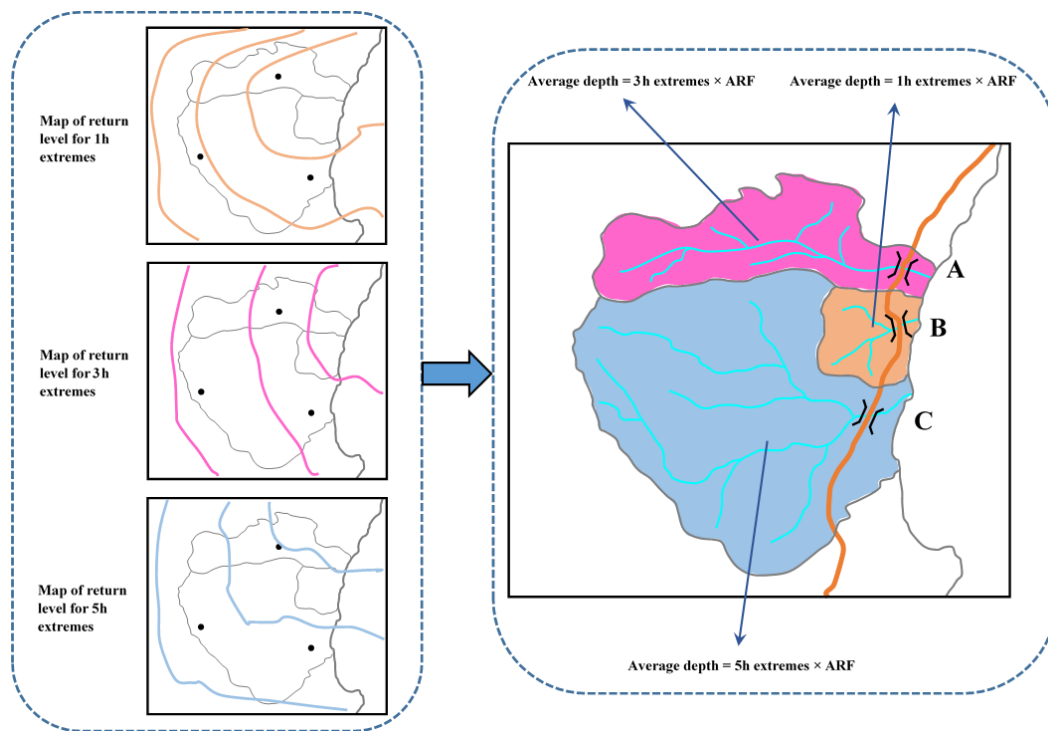


140
 141 **Figure 1.** Illustration of process to estimate rainfall extremes for each individual location in conventional flood risk
 142 approach, the upper panel is for gauge 1 and the lower panel is for gauge 2.

143 Having obtained the IDF estimates for individual locations in Fig. 1, the next step is commonly to
 144 convert this to spatial IDF maps by interpolating results between gauged locations. Figure 2 shows
 145 hypothetical IDF maps from individual sites, with a separate spatial contour map usually provided for
 146 each storm burst duration. In a conventional application the respective maps are used to estimate the
 147 magnitude of extreme rainfall over catchments for a specified time of concentration. The IDF estimates
 148 are combined with an areal reduction factor (ARF) to determine the volume of rainfall over a region
 149 (since rainfall is not simultaneously extreme at all locations over the region). However, because the
 150 spatial dependence was broken in the IDF analysis, the ARFs come from a separate analysis and are an
 151 attempt to correct for the broken spatial relationship within a catchment (Bennett et al., 2016a). Lastly,
 152 the rainfall volume over the catchment is combined with a temporal pattern (i.e. the distribution of the

153 rainfall hyetograph within a single ‘storm burst’) and input to a runoff model to simulate flood-flow at
 154 a catchment’s outlet. Where catchment flows can be considered independently this process has been
 155 acceptable for conventional design, but because this process does not account for dependence across
 156 durations and across a region, it is not possible to address problems that span multiple catchments, as
 157 with civil infrastructure systems.

158



159

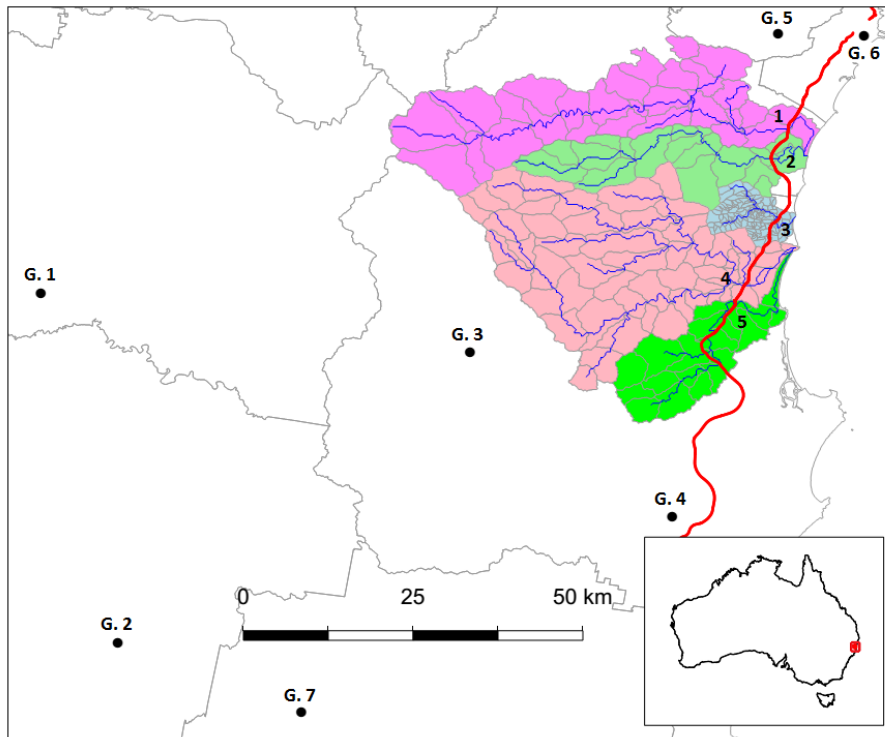
160 **Figure 2.** Illustration of map of return level and how to use it in estimating flood flow in conventional flood risk estimates
 161 approach.

162 The process in Fig. 1 breaks out the dependence of the observed rainfall, which makes the conventional
 163 approach unable to analyse the dependence of flooding at two or more separate locations. Instead, this
 164 paper advocates for spatially dependent IDF estimates that are developed by retaining the dependence
 165 of observed rainfall in the estimation of extremal rainfall. By applying spatially dependent IDF
 166 estimates to a rainfall-runoff model, it becomes possible to represent the dependence of flooding
 167 between separate locations.

168 **3. Case study and data**

169 The region chosen for the case study is in the mid north coast region of New South Wales, Australia.
170 This region has been the focus of a highway upgrade project and has an annual average daily traffic
171 volume on the order of 15,000 vehicles along the existing highway. The upgrade traverses a series of
172 coastal foothills and floodplains for a total length of approximately 20 km. The project's major river
173 crossings consist of extensive floodplains with some marsh areas.

174 The case study has five main catchments that are numbered in sequence in Fig. 3: (1) Bellinger, (2)
175 Kalang River, (3) Deep Creek, (4) Nambucca and (5) Warrell Creek. The area and time of concentration
176 of these catchments is summarised in Table 1, with the latter estimated using the ratio of the flow path
177 length and average flow velocity ([SKM, 2011](#)). The Deep Creek catchment has a time of concentration
178 of 8 hr, while the other four catchments have much longer times of concentration, ranging from 27 to
179 38 hr. The differing durations indicate that it is necessary to consider spatial dependence across this
180 range of durations to estimate joint and conditional flood risk. The spatial dependence across rainfall
181 durations is expected to be lower than across a single duration, since short- and long-rain events are
182 often driven by different meteorological mechanisms ([Zheng et al., 2015](#)). However some spatial
183 dependence is still likely to be present, given that extremal rainfall in the region is strongly associated
184 with 'east coast low' systems off the eastern coastline, whereby extreme hourly rainfall bursts are often
185 embedded in heavy multi-day rainfall events.



186

187 **Figure 3.** Map of the case study in New South Wales, Australia. The black dots indicate the rainfall gauges (G. 1 to G. 7),
 188 the red line indicates the Pacific Highway upgrade project, and the blue lines indicate the main river network. The numbers
 189 from one to five indicate the locations of the main river crossings.

190

Table 1. Summary of case study catchments properties-

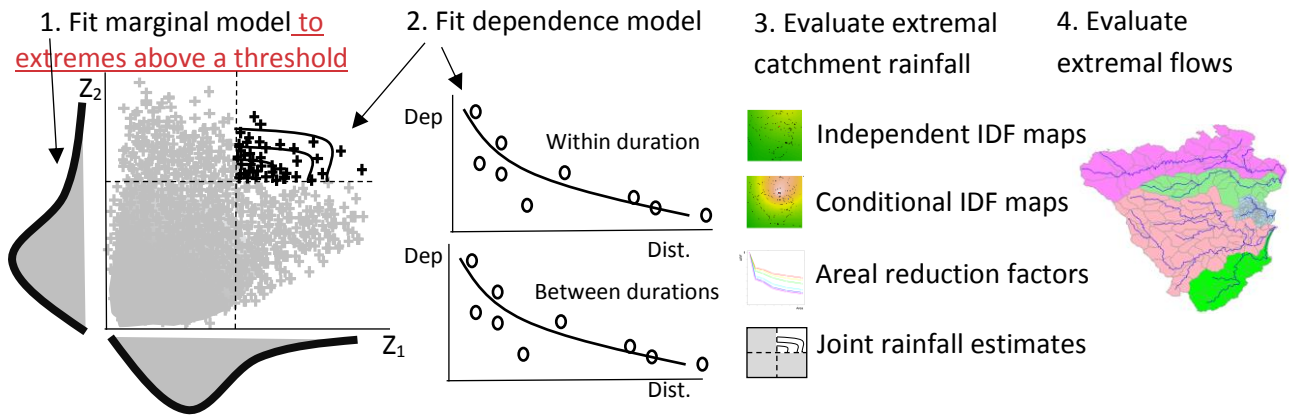
No.	Catchment	Area (km ²)	Time of concentration (hour)
1	Bellinger	772	37
2	Kalang River	341	33
3	Deep Creek	92	8
4	Nambucca (upper)	1020	38
5	Warrell Creek	294	27

191 The black circles in Fig. 3 represent the sub-daily rain stations used for this study. There were seven
 192 sub-daily stations selected, with 35 years of record in common for the whole region. The data was
 193 available at a 5 minute interval and aggregated to longer durations. For convenience in comparing the
 194 times of concentration between the catchments, this study assumes a time of concentration of 9 hr for
 195 the Deep Creek catchment, while identical times of concentration of 36 hr are assumed for the other
 196 four catchments.

197

198 **4. Methodology**

199 This section describes the method used to estimate the conditional and joint probabilities of streamflow
 200 for civil infrastructure systems based on rainfall extremes, with the sequence of steps illustrated in Fig.
 201 4. The overall aim is to estimate rainfall exceedance probabilities and corresponding flow estimates that
 202 account for dependence across multiple catchments. The generalized Pareto distribution (GPD) is used
 203 as the marginal distribution to fit to observed rainfall above some large threshold for all durations at
 204 each location (Section 4.1). An extremal dependence model is required to evaluate conditional and joint
 205 probabilities. Here, an inverted max-stable process is used with dependence not only in space but also
 206 in duration (Section 4.2). The fitted model is evaluated in a range of contexts, including the construction
 207 of joint and conditional return level maps. The derivation of areal reduction factors and joint rainfall
 208 estimates are made with the assistance of simulations based on the fitted model (Section 4.3). An event-
 209 based rainfall-runoff model is employed in Section 4.4 to transform extremal design rainfalls to
 210 corresponding flows.



211

212 **Figure 4.** The flow chart for the overall methodology.

213 **4.1. Marginal model for rainfall**

214 This study defines extremes as those greater than some threshold u . For large u , the distribution of Y
 215 conditional on $Y > u$ may be approximated by the generalized Pareto distribution (GPD) (Pickands,
 216 1975; Davison and Smith, 1990; Thibaud et al., 2013):

217
$$G(y) = 1 - \left\{ 1 + \frac{\xi(y - u)}{\sigma_u} \right\}^{-1/\xi}, \quad y > u, \quad (1)$$

218 defined on $\{y: 1 + \xi(y - u)/\sigma_u > 0\}$ where $\sigma_u > 0$ and $-\infty < \xi < +\infty$ are scale and shape
219 parameters, respectively. The probability that a level y is exceeded is $\Phi_u\{1 - G(y)\}$, where $\Phi_u =$
220 $\Pr(Y > u)$.

221 The selection of the appropriate threshold u involves a trade-off between bias and variance. A threshold
222 that is too low leads to bias because the GPD approximation is poor. A threshold too high leads to high
223 variance because of a small number of excesses. Two diagnostic tests are used to determine the
224 appropriate threshold u : the mean residual life plot and the parameter estimate plot (Coles, 2001;
225 Davison and Smith, 1990). These methods use the stability property of a GPD, so that if a GPD is valid
226 for all excesses above u , then excesses of a threshold greater than u should also follow a GPD (Coles
227 (2001). To construct IDF maps across the region, the parameters of the GPD are interpolated across the
228 region using a thin plate spline with covariates of longitude and latitude. Though more detailed
229 modelling of covariates could be used to improve estimates (Le et al. (2018b), the interpolation used
230 here is sufficient for demonstrating the overall method.

231 **4.2. Dependence model for spatial rainfall**

232 Consider rainfall as a stationary stochastic process Z_i associated with a location x_i and a specific
233 duration (the notation is simplified from $Z(x_i)$ to Z_i). An important property of dependence in the
234 extremes is whether or not two variables are likely/unlikely to co-occur as the extremes become rarer,
235 as this can significantly influence the estimate of frequency for flood events of large magnitude. This
236 is referred to as asymptotic dependence/independence, respectively. For the case of asymptotic
237 independence, the dependence structure becomes weaker as the extremal threshold increases, which is
238 defined as $\lim_{z \rightarrow \infty} P\{Z_1 > z | Z_2 > z\} = 0$ for all $x_1 \neq x_2$. The spatial extent of a rainfall event with
239 asymptotically independent extremes will diminish as its rarity increases. This study uses an
240 asymptotically independent model, of which ~~multiple there are multiple~~ types are valid including the
241 Gaussian copula (Davison et al., 2012) and inverted max-stable processes (Wadsworth and Tawn,
242 2012). The inverted max-stable model was ultimately selected in this study to provide consistency
243 earlier research (Le et al., 2018a), in which it was demonstrated to preserve the spatial properties of
244 extreme rainfall in an Australian context, including the property of asymptotic independence. Thibaud

et al. (2013) also compared the inverted max-stable model with a Gaussian copula in a case study in Switzerland, and identified that the inverted max-stable model was appropriate. This study uses an inverted Brown-Resnick max-stable process (Asadi et al., 2015; Huser and Davison, 2013; Kabluchko et al., 2009; Oesting et al., 2017) used on a performance evaluation summarised in Le et al. (2018a).

The dependence structure of the inverted max-stable process is represented by the pairwise residual tail dependence coefficient (Ledford and Tawn, 1996). For a generic continuous process Z_i for a given duration and associated with a specific location x_i , the empirical pairwise residual tail dependence coefficient η for each pair of locations (x_1, x_2) is

$$\eta(x_1, x_2) = \lim_{z \rightarrow \infty} \frac{\log P\{Z_2 > z\}}{\log P\{Z_1 > z, Z_2 > z\}}. \quad (2)$$

The value of $\eta \in (0,1]$ indicates the level of extremal dependence between Z_1 and Z_2 (Coles et al., 1999), with lower values indicating lower dependence. An example of how to calculate the residual tail dependence coefficient is provided in Appendix A for a sample dataset. To estimate the dependence structure of an inverted max-stable model, the theoretical residual tail dependence coefficient function is fitted to its empirical counterpart. Here the residual tail dependence coefficient function is assumed to only depend on the Euclidean distance between two locations $h = \|x_1 - x_2\|$. The theoretical residual tail dependence coefficient function for the inverted Brown-Resnick model is given as:

$$\eta(h) = \frac{1}{2\Phi\left\{\sqrt{\frac{\gamma(h)}{2}}\right\}}, \quad (3)$$

where Φ is the standard normal cumulative distribution function, h is the distance between two locations, and $\gamma(h)$ belongs to the class of variograms $\gamma(h) = \|h\|^\beta/q$ for $q > 0$ and $\beta \in (0,2)$. The model is fitted to the empirical residual tail dependence coefficient by modifying parameters q and β until the sum of squared errors is minimized.

~~The inverted max-stable process is fitted to the observations by minimizing the sum of the squared errors of the residual tail dependence coefficients.~~ When the extreme rainfall at location x_1 and x_2 are of different durations, the dependence is less than when the extremes are of the same duration. For

269 example, at a single location ($h = 0$), when the duration is the same, the rainfall values are identical and
270 have perfect dependence, but when the duration of extremes are different the values are not identical
271 and the dependence is less. An adjustment needs to be made to the theoretical pairwise residual tail
272 dependence coefficient function when extreme rainfalls have different durations.

273 Following [Le et al. \(2018b\)](#), an adjusted approach is used by adding a nugget to the variogram as:

$$274 \quad \gamma_{ad.}(h) = h^\beta/q + c(D - d)/d, \quad (4)$$

275 where h , β , and q are the same as those in Eq. (3); d is the duration (in hours); $0 < d \leq D$, where D is
276 the maximum duration of interest (e.g. $D = 36$ hr for the case study described in this paper); and c is
277 a parameter to adjust dependence according to duration. This adjustment is intended to condition the
278 behaviour of shorter duration extremes on a D -hour extreme of specified magnitude. It is constructed
279 to reflect the fact that when compared to a D -hour extreme, a shorter duration results in less extremal
280 dependence. Cases involving conditioning of longer periods on shorter periods (such as a 36 hr extreme
281 given a 9 hr extreme has occurred) can also use the relationship in Eq. (4), but with different parameter
282 values.

283 To fit the inverted max-stable process for all pairs of durations at locations x_1 and x_2 (i.e. 36 hr and 12
284 hr, 36 hr and 9 hr, 36 hr and 6 hr, 36 hr and 2 hr, 36 hr and 1 hr), the theoretical pairwise residual tail
285 dependence coefficient function in Eq. (3) is used with the adjusted variogram from Eq. (4) where the
286 parameters β and q are first obtained from the fitted results of the case of identical 36 hr durations at
287 location x_1 and x_2 . The parameter c is obtained by a least square fit of the residual tail dependence
288 coefficient across all durations.

289 ***4.3. Simulation based estimation of areal and joint rainfall***

290 The dependence model specification in the previous section enables the calculation of joint and
291 conditional probabilities (Appendix B). Therefore, in addition to traditional IDF return level maps that
292 are based on independence between locations and durations, it is possible to account for the coincidence
293 of rainfall within the region. Current design procedures using IDF estimates are event-based and rely
294 on ancillary steps to reconstruct elements of the design storm that were broken during the estimation

295 procedure. One critical element is the areal reduction factor (ARF), which [can also be estimated by](#)
296 [using](#) the dependence model ~~can also be used to estimate~~. ARFs are used to adjust rainfall at a point
297 (such as the centroid of a catchment) to an effective mean rainfall over the catchment with equivalent
298 probability of exceedance ([Ball et al., 2016](#); [Le et al., 2018a](#)). ARFs can be estimated from observed
299 rainfall data, but it is difficult to extrapolate them for long return periods from observations with just
300 35 years of record for this study. To deal with this difficulty and to analyse the asymptotic behaviour
301 of ARFs, [Le et al. \(2018a\)](#) proposed a framework to simulate ARFs using the same inverted-max stable
302 process model adopted here. The simulation procedure from [Le et al. \(2018a\)](#) is summarised according
303 to two steps. In the first step, the theoretical residual tail dependence coefficient function in Eq. (3) is
304 fitted to observed rainfall for the duration of interest to obtain the variogram parameters $q > 0$ and $\beta \in$
305 $(0,2)$. The inverted Brown-Resnick process is obtained from a simulation of the Brown-Resnick process
306 using the algorithm of [Dombry et al. \(2016\)](#) over a spatial domain. In the second step, the simulation in
307 step 1 is transformed from unit Fréchet margins to the rainfall scaled margins (inverse transformation
308 of Eq. (B.1) in Appendix B). For rainfall magnitudes above the threshold the generalised Pareto
309 distribution in Eq. (1) is used, and below the threshold the empirical distribution is used. The empirical
310 distributions at ungauged sites are derived from the nearest gauged sites and using the interpolated
311 response surface of the GPD threshold parameter.

312 An advantage of the simulation approach is that it can reflect the proportion of dry days in the empirical
313 distribution by making the simulated rainfall contain zero values ([Thibaud et al., 2013](#)). Another
314 advantage is that the use of empirical distributions guarantees that the marginal distributions of
315 simulated rainfall below the threshold match the observed marginal distributions. There may be a
316 drawback by forcing the simulated rainfall to have the same extremal dependence structure for both
317 parts below and above the threshold, which may not be true for non-extreme rainfall. However, the
318 dependence structure of non-extreme rainfall contributes insignificantly to extreme events ([Thibaud et](#)
319 [al., 2013](#)) and is unlikely to affect the results.

320 For calculating ARFs, the simulation is implemented separately for spatial rainfall of 36 and 9 hrs
321 duration. ARFs are calculated for each duration and different return periods, which can be found in the

322 supplementary material (Fig. S1 and S2). Figure S1 and S2 provide relationships between ARFs and
323 area (in km²) for different return periods for the case study catchments simulated using the inverted
324 Brown-Resnick process over equally sized grid points. The relationships are interpolated to obtain the
325 ARFs for each subcatchment.

326 The recommended approach for estimating the overall failure probability of a system is demonstrated
327 by considering a hypothetical traffic system with multiple river crossings at locations. If there is a one-
328 to-one correspondence between extreme rainfall intensity over a catchment and flood magnitude, the
329 overall failure probability will be approximately equal to the probability that there is at least one river
330 crossing whose contributing catchment has rainfall extremes exceeding the design level, which can be
331 estimated using simulations of the spatial rainfall model. Given the different times of concentration in
332 each catchment, the simulation must account for extremes of different durations. Specifically, the
333 covariance matrix of the simulation procedure provided by [Dombry et al. \(2016\)](#) is calculated from the
334 variogram in Eq. (3). The covariance element for a pair of locations with the same duration (e.g. 36 and
335 36 hr) is calculated from the variogram of identical durations for 36 and 36 hr. The covariance element
336 for a pair of locations with different durations, for example 36 and 9 hr, is calculated from the variogram
337 across durations for 36 and 9 hr. A set of 10,000 years simulated rainfall is generated from the fitted
338 model to calculate the overall failure probability of a highway section (Eq. B.5). The process is repeated
339 100 times to estimate the average failure probability, under the assumption that all river crossings of
340 the highway are designed to the same individual failure probability.

341 ***4.4. Transforming rainfall extremes to flood flow***

342 To estimate flood flow from rainfall extremes, the Watershed Bounded Network Model (WBNM)
343 ([Boyd et al., 1996](#)), is employed. WBNM calculates flood runoff from rainfall hyetographs that
344 represent the relationship between the rainfall intensity and time ([Chow et al., 1988](#)). It divides the
345 catchment into subcatchments, allowing hydrographs to be calculated at various points within the
346 catchment, and allowing the spatial variability of rainfall and rainfall losses to be modelled. It separates
347 overland flow routing from channel routing, allowing changes to either or both of these processes, for
348 example in urbanised catchments. The rainfall extremes are estimated at the centroid of the catchment,

349 and are converted to average spatial rainfall using the simulated ARFs described in Section 4.3. Design
350 rainfall hyetographs are used to convert the rainfall magnitude to absolute values through the duration
351 of a storm following standard design guidance in Australia ([Ball et al., 2016](#)).

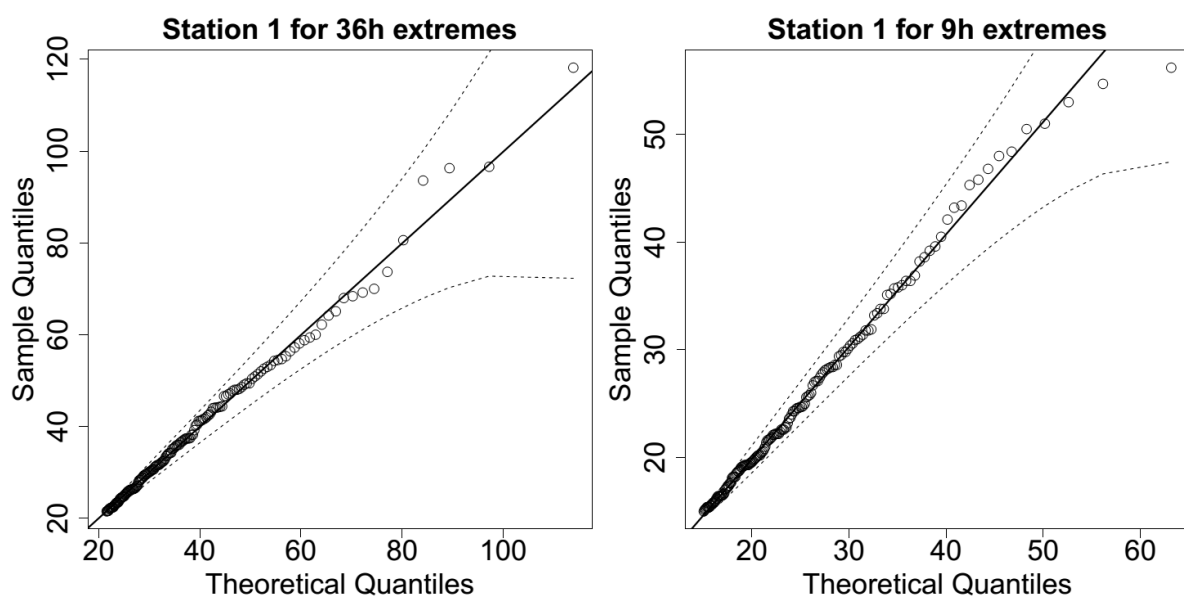
352 Hydrological models (WBNM) for the case study area were developed and calibrated in previous
353 studies ([WMAWater, 2011](#)). Hydrological model layouts for the Bellinger, Kalang River, Nambucca,
354 Warrell and Deep Creek catchments can be found in the supplementary material (Fig. S3 to S5).

355 5. Results

356 5.1. Evaluation of model for space-duration rainfall process

357 A GPD with an appropriate threshold was fitted to the observed rainfall data for 36 hr and 9 hr durations,
358 and the Brown-Resnick inverted max-stable process model was calibrated to determine the spatial
359 dependence.

360 Analysis of the rainfall records led to the selection of a threshold of 0.98 for all records as reasonable
361 across the spatial domain and the GPD was fitted to data above the selected threshold. Figure 5 shows
362 QQ plots of the marginal estimates for a representative station for two durations (36 and 9 hr). Overall
363 the quality of fitted distributions is good and plots for all other stations can be found in the
364 supplementary material (Fig. S6 and S7).

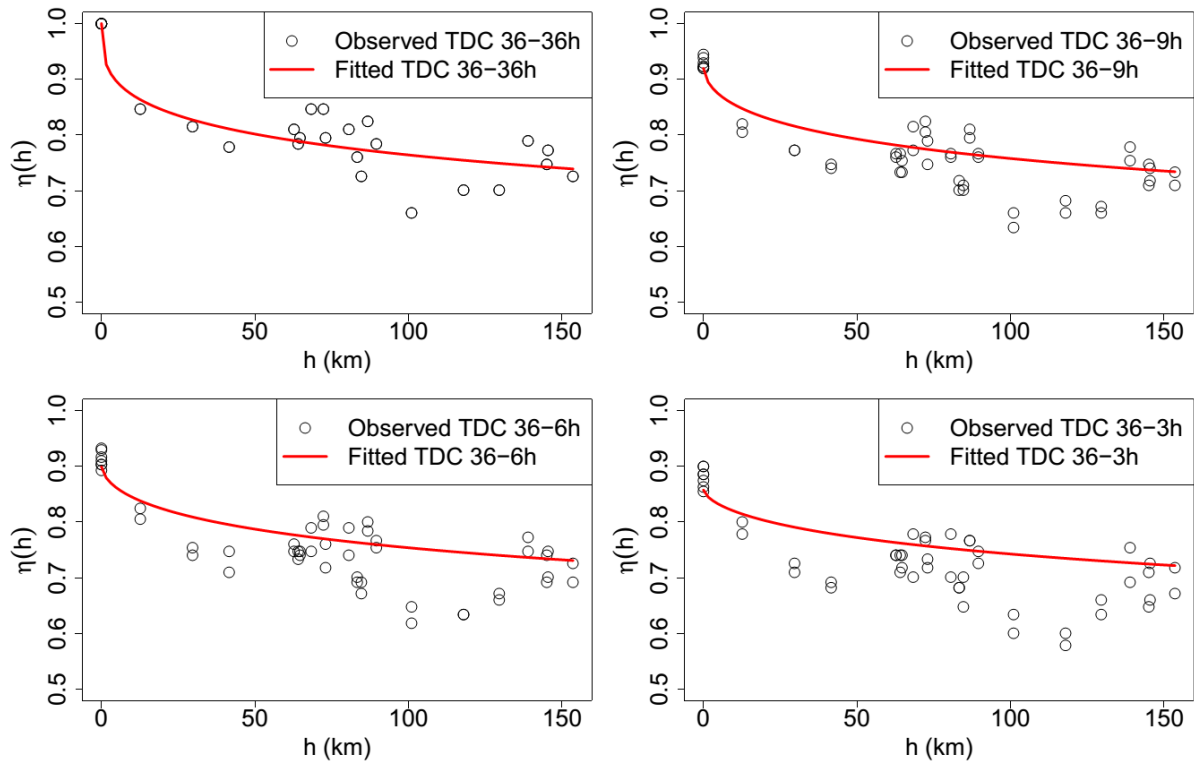


365

366 **Figure 5.** QQ plots for the fitted GPD at one representative station, dotted lines are the 95% confidence bounds, and the
367 solid diagonal line indicates a perfect fit.

368 The inverted max-stable process across different durations was calibrated to determine dependence
369 parameters. The theoretical pairwise residual tail dependence coefficient function between two
370 locations (x_1 and x_2) was calculated based on Eq. (3) and Eq. (4), and the observed pairwise residual
371 tail dependence coefficient η was calculated using Eq. (2). Figure 6 shows the pairwise residual tail
372 dependence coefficients for the Brown-Resnick inverted max-stable process versus distance. The black
373 points are the observed pairwise residual tail dependence coefficients, while the red lines are the fitted
374 pairwise residual tail dependence coefficient functions. A coefficient equal to 1 indicates complete
375 spatial dependence, and a value of 0.5 indicates complete spatial independence. The top-left panel
376 shows the dependence between 36 hr extremes across space, with the distance $h = 0$ corresponding to
377 “complete dependence”. It also shows the dependence decreasing with increasing distance. Figure 6
378 indicates that the model has a reasonable fit to the observed data given the small number of dependence
379 parameters. Although the theoretical coefficient (red line) does not perfectly match at long distances,
380 the main interest for this case study is in short distances, including at $h = 0$ for the case of dependence
381 between two different durations at the same location.

382 The remaining panels of Fig. 6 show the dependence of 36 vs. 9 hr extremes, 36 vs. 6 hr extremes, and
383 36 vs. 3 hr extremes, with the latter two duration combinations not being used directly in the study but
384 nonetheless showing the model performance across several durations. As expected, the dependence
385 levels are weaker compared with 36 vs. 36 hr extremes at the same distance, especially at zero distance.
386 This is expected, as extremes of different durations are more likely to arise from different storm events
387 compared to storms of the same duration.



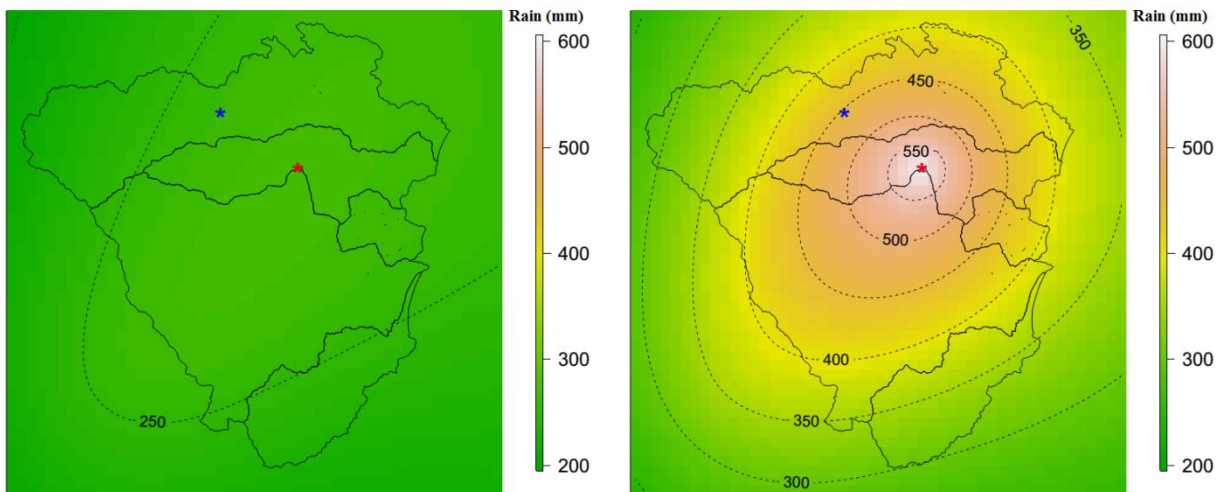
388

389 **Figure 6.** Plots of pairwise residual tail dependence coefficient (TDC) against distance for 36 hr extremes and 36 hr
 390 extremes (top left), for 36 hr extremes and 9 hr extremes (top right), for 36 hr extremes and 6 hr extremes (bottom left), and
 391 for 36 hr extremes and 3 hr extremes (bottom right). The black points are estimated residual tail dependence coefficients for
 392 pairs of sub-daily stations, and the red lines are theoretical residual tail dependence coefficient function.

393 **5.2. Estimating conditional rainfall return levels and corresponding conditional flows for evacuation**
 394 **route design**

395 The recommended approach for estimating conditional rainfall extremes is demonstrated by considering
 396 a hypothetical evacuation route across location x_2 , given a flood occurs at location x_1 , evaluated using
 397 Eq. (B.4). This approach is applied to a case study of the Pacific Highway upgrade project that contains
 398 five main river crossings (from Fig. 3). For evacuation purposes, we need to know “what is the
 399 probability that a bridge fails only once on average every M times (e.g., $M = 10$ for a one in 10 chance
 400 conditional event) when a neighbouring bridge is flooded?” This section provides the conditional
 401 estimates for two pairs of neighbouring bridges in the case study that have the shortest Euclidean
 402 distances, i.e. pairs (x_1, x_2) and (x_2, x_3) . The comparisons of unconditional and conditional maps are
 403 given in Fig. 7 and Fig. 8, and the corresponding unconditional and conditional flows are given in Fig.
 404 9.

405 The left panel of Fig. 7 provides the pointwise 10-year unconditional return level map over the case
 406 study area for 36 hr rainfall extremes. The value at the location of interest—the blue star (the centroid
 407 of Bellinger catchment)—is around 260 mm. The right panel of Fig. 7 indicates that when accounting
 408 for the effect of a 20-year event for 36 hr rainfall extremes happening at the location of the red star (the
 409 centroid of Kalang River catchment), the pointwise one in 10 chance conditional return level at the blue
 410 star rises to around 453 mm (i.e., 1.74 times the unconditional value).

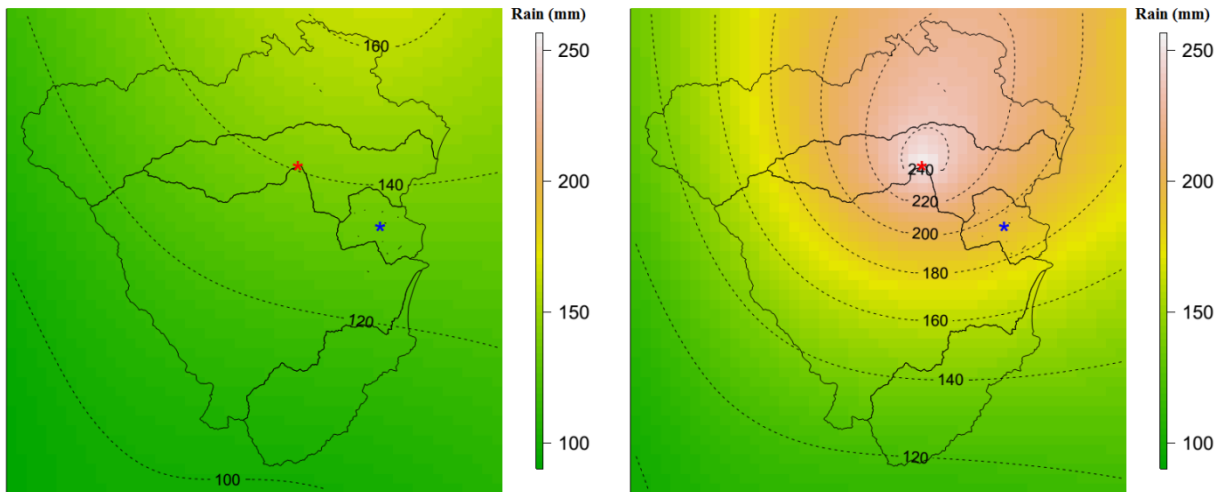


411

412 **Figure 7.** Pointwise 10-year unconditional return level map (mm) for 36 hr extremes (left), and pointwise one in 10 chance
 413 conditional return level map (mm) for 36 hr extremes given a 20-year event for 36 hr extremes happen at location of the red
 414 star for the centroid of Kalang River catchment (right). The colour scales are the same for comparison.

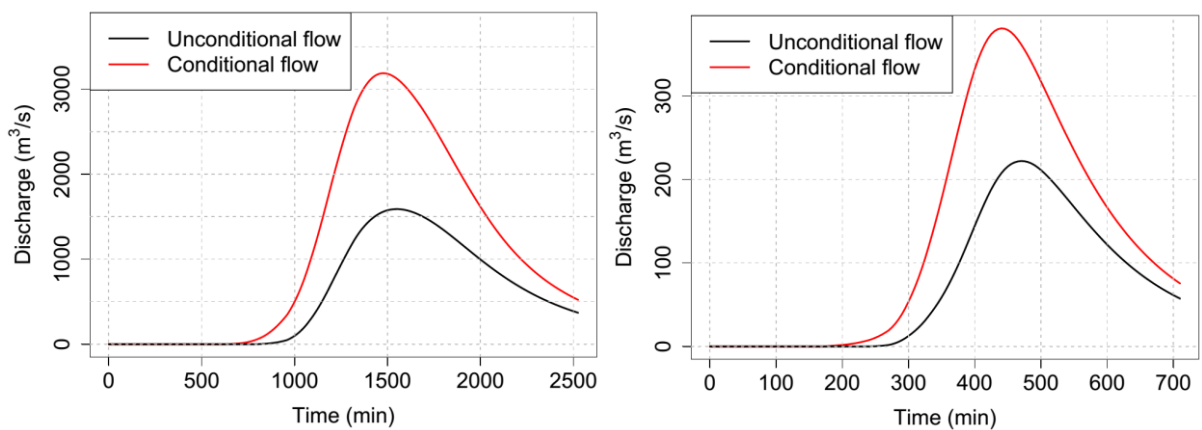
415 Figure 8 provides similar plots to Fig. 7 for another pair of locations having different durations of
 416 rainfall extremes due to different times of concentration in each catchment. Here, the location of interest
 417 is the centroid of the Deep Creek catchment (the blue star in Fig. 8) and the conditional point is the
 418 centroid of the Kalang River catchment (the red star in Fig. 8). The pointwise 10-year unconditional
 419 and one in 10 chance conditional return levels at the location of the blue star are 134 mm and 194 mm,
 420 respectively. The relative difference between the conditional and unconditional return levels is only
 421 1.45 times, compared with 1.74 times for the case in Fig. 7. This is because the pair of locations in Fig.
 422 8 has a longer distance than those in Fig. 7, so that the dependence level is weaker. Moreover, the
 423 location pair in Fig. 8 was analysed for different durations (between 36 and 9 hr extremes), which has

424 weaker dependence than the case of the equivalent durations in Fig. 7 (between 36 and 36 hr), based on
 425 Fig. 6.



426
 427 **Figure 8.** Pointwise 10-year unconditional return level map (mm) for 9 hr extremes (left), and pointwise one in 10 chance
 428 conditional return level map (mm) for 9 hr extremes, given a 20-year event for 36 hr extremes happens at location of the red
 429 star for the centroid of the Kalang River catchment (right). The colour scales are the same for comparison.

430 The unconditional and conditional return levels were extracted at the centroid of each main catchment,
 431 and were converted to the absolute values of rainfall using a corresponding ARF and design storm
 432 hyetograph. The unconditional and conditional flood flows at the river crossing in the Bellinger
 433 catchment (corresponding to the unconditional and conditional rainfall extremes in Fig. 7) are given in
 434 Fig. 9 (left panel). Similar plots for the river crossing in the Deep Creek catchment (corresponding to
 435 the unconditional and conditional rainfall extremes in Fig. 8) are given in Fig. 9 (right panel).



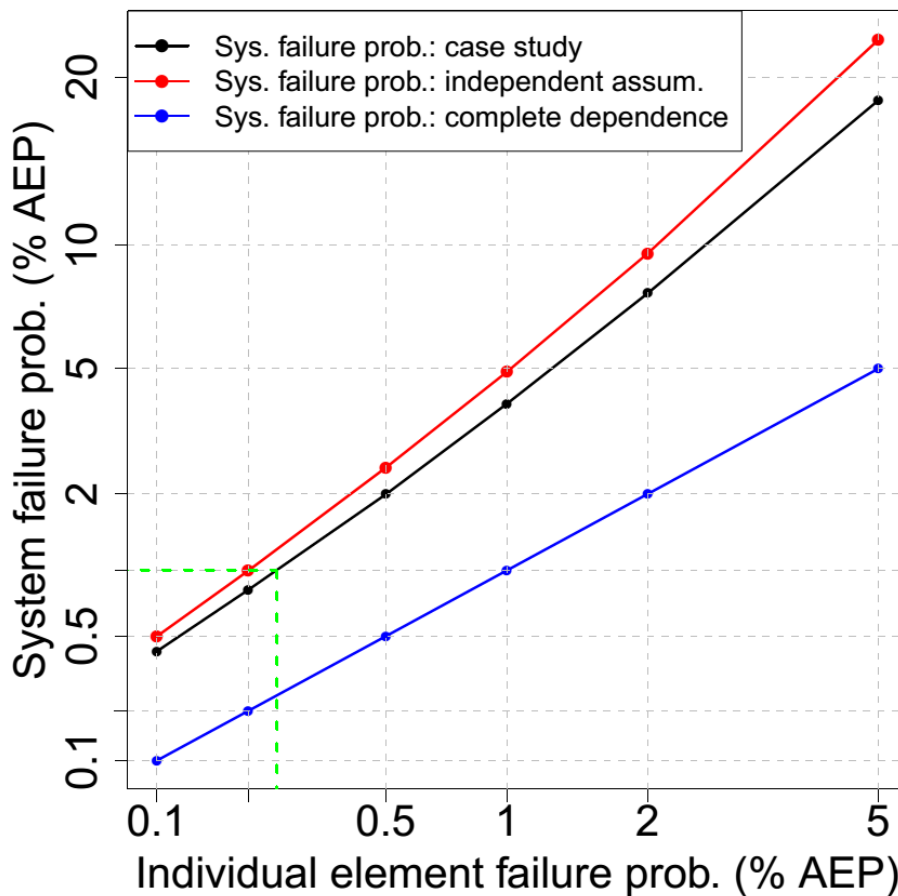
437 **Figure 9.** Comparison between conditional flows (red line) and unconditional flows (black line). (left) At the river crossing
438 in the Bellinger catchment (number 1 in Figure 3): conditional flow caused by an one in 10 chance conditional event for 36
439 hr rainfall in considering the effect of a 20-year event for 36 hr rainfall occurring at the river crossing in the Kalang River
440 catchment, and unconditional flow caused by a 10-year unconditional event for 36 hr. (right) At the river crossing in the
441 Deep Creek catchment (number 3 in Figure 3): conditional flow caused by an one in 10 chance conditional event for 9 hr
442 rainfall in considering the effect of a 20-year event for 36 hr rainfall occurring at the river crossing in the Kalang River
443 catchment, and unconditional flow caused by a 10-year unconditional event for 9 hr rainfall.

444 Fig. 9 presents peak flow for the Bellinger (left panel) and Deep Creek (right panel) catchments,
445 indicating that the peak conditional flow at the river crossings is almost 2.0 and 1.7 times higher than
446 the unconditional flow for the two catchments, respectively. This difference is a direct result of the
447 conditional event having a higher rainfall magnitude than the unconditional event: given that there is
448 an extreme event nearby, it is more likely for an extreme event to occur at a nearby location. If a bridge
449 design were to take into account this extra criterion for the purposes of evacuation planning it would
450 require the design to be at a higher level.

451 *5.3. Estimating the failure probability of the highway section based on the joint probability of rainfall* 452 *extremes*

453 Figure 10 is a plot of the overall failure probability of the highway as a function of the failure probability
454 of each individual river crossing (black). Similar relationships for the cases of complete dependence
455 (blue) and independence (red) are also provided for comparison. For the case of complete dependence,
456 when the whole region is extreme at the same time, the overall failure probability of the highway is
457 equal to the individual river crossing failure probability and it represents the lowest overall failure
458 probability. The worst case is complete independence where extremes do not happen together unless by
459 random chance; this means the failure probability of the highway is much higher than that for individual
460 river crossings. Taking into account the real dependence, there are some extremes that align and it seems
461 from Fig. 10 that this is a relatively weak effect. As an example from Fig. 10, to design the highway
462 with a failure probability of 1% annual exceedance probability (AEP), we would have to design each
463 individual river crossing to a much rarer AEP of 0.25% (see green lines in Fig. 10).

464



466

467 **Figure 10.** Relationship between system failure probability and individual element failure probability in % annual
 468 exceedance probability (% AEP). The black colour is for the case study, the red colour is for the case of independence, and
 469 the blue colour is for the case of complete dependence. The green lines help to interpolate the individual element failure
 470 probability from a given system failure probability of 1%. Both horizontal axis and vertical axis are constructed at a double
 471 log scale for viewing purposes.

472 6. Discussion and Conclusions

473 Hydrological design that is based on IDF estimates has conventionally focussed on separate estimation
 474 at single locations. Such an approach can lead to the misspecification of wider system risk of flooding
 475 since weather systems exhibit dependence in space, time and across storm durations, which can lead to
 476 the coincidence of extremes. A number of methods have been developed to address the problem of
 477 antecedent moisture within a single catchment, by accounting for the temporal dependence of rainfall
 478 at locations of interest through loss parameters or sampling rainfall patterns (Rahman et al., 2002).
 479 However, there have been fewer methods that account for the spatial dependence of rainfall across

480 multiple catchments, due in part to the complexity of representing the effects of spatial dependence in
481 risk calculations. Different catchments can have different times of concentration, so spatial dependence
482 may also imply the need to consider dependence across different durations of extreme rainfall bursts.

483 Recent and ongoing advances in modelling spatial rainfall extremes provide an opportunity to revisit
484 the scope of hydrological design. Such models include a max-stable model fitted using a Bayesian
485 hierarchical approach ([Stephenson et al., 2016](#)), max-stable and inverted max-stable models ([Nicolet et](#)
486 [al., 2017](#); [Padoan et al., 2010](#); [Russell et al., 2016](#); [Thibaud et al., 2013](#); [Westra and Sisson, 2011](#)) and
487 latent-variable Gaussian models ([Bennett et al., 2016b](#)). The ability to simulate rainfall over a region
488 means that hydrological problems need not be confined to individual catchments, but may cover
489 multiple catchments. Civil infrastructure systems such as highways, railways or levees are such
490 examples, since the failure of any one element may lead to overall failure of the system. Alternatively,
491 where there is a network, the failure of one element may have implications for the overall system to
492 accommodate the loss, by considering alternative routes. With models of spatial dependence and
493 duration dependence of extremes, there is a new and improved ability to address these problems
494 explicitly as part of the design methodology.

495 This paper demonstrated an application for evaluating conditional and joint probabilities of flood at
496 different locations. This was achieved with two examples: (i) the design of a river crossing that will fail
497 once on average every M times given that its neighbouring river crossing is flooded; and (ii) estimating
498 the probability that a highway section, which contains multiple river crossings, will fail based on the
499 failure probability of each individual river crossing. Due to the lack of continuous streamflow data and
500 sub-daily limitations of rain-based continuous simulation, this study used an event-based method of
501 conditional and joint rainfall extremes to estimate the corresponding conditional and joint flood flows.

502 The spatial rainfall was simulated using an asymptotically independent model, which was then used to
503 estimate conditional and joint rainfall extremes. Although this study focused on the inverted max-stable
504 model to simulate the extreme rainfall process, other methods such as the Gaussian copula may also be
505 appropriate and should be considered in future applications.

506 An empirical method was obtained from the framework of [Le et al. \(2018b\)](#) to make an asymptotically
507 independent model—the inverted max-stable process—able to capture the spatial dependence of rainfall
508 extremes across different durations. The fitted residual tail dependence coefficient function showed that
509 the model can capture the dependence for different pairs of durations. For our example, the highest ratio
510 of the one in 10 chance conditional event (in considering the effect of a 20-year event rainfall occurring
511 at the conditional location) to the 10-year unconditional event was 1.74, for the two catchments having
512 the strongest dependence (Fig. 7). The corresponding conditional flows were then estimated using a
513 hydrological model WBNM and shown to be strongly related to the ratio of conditional and
514 unconditional rainfall extremes (Fig. 9).

515 The joint probability of rainfall extremes for all catchments and for all possible pairs of catchments in
516 the case study area was estimated empirically from a set of 10,000 years of simulated rainfall extremes,
517 repeated 100 times to estimate the average value. The results showed that there were differences in the
518 failure probability of the highway after taking into account the rainfall dependence, but the effect was
519 not as emphatic as with the case of conditional probabilities. The difference in the failure probability
520 became weaker as the return period increased, which is consistent with the characteristic of
521 asymptotically independent data ([Ledford and Tawn, 1996](#); [Wadsworth and Tawn, 2012](#)). A
522 relationship was demonstrated (Fig. 10) to show how the design of the overall system to a given failure
523 probability requires the design of each individual river crossing to a rarer extremal level than when each
524 crossing is considered in isolation. For the case study example, it would be necessary to design each of
525 the five bridges to a 0.25% AEP event in order to obtain a system failure probability of 1%.

526 There is a need to reimagine the role of intensity-duration-frequency relationships. Conventionally they
527 have been developed as maps of the marginal rainfall in a point-wise manner for all locations and for a
528 range of frequencies and durations. The increasing sophistication of mathematical models for extremes,
529 computational power and interactive graphics abilities of online mapping platforms means that analysis
530 of hydrological extremes could significantly expand in scope. With an underlying model of spatial and
531 duration dependence between the extremes, it is not difficult to conceive of digital maps that
532 dynamically transform from the marginal representation of extremes to the corresponding

533 representation conditional extremes after any number of conditions are applied. This transformation is
534 exemplified by the differences between left and right panels in Fig. 7 and Fig. 8. Enhanced IDF maps
535 would enable a very different paradigm of design flood risk estimation, breaking away from analysing
536 individual system elements in isolation and instead emphasizing the behaviour of entire system.

537 **Appendix A. Calculation of empirical tail dependence coefficient**

538 To illustrate how Eq. (2) in the manuscript is calculated, consider a set of $n = 10$ observed values at
 539 the two locations: Z_1 and Z_2 (see Table A1). First, Z_1 and Z_2 are converted to empirical cumulative
 540 probability estimates via the Weibull plotting position formula $P = j/(n + 1)$ where j is ranked index
 541 of a data point giving P_1 and P_2 (see Table A1).

542 **Table A1.** Observed data Z_1 and Z_2 and corresponding empirical cumulative probabilities P_1 and P_2 .

Z_1	Z_2	P_1	P_2
5	10	0.455	0.909
9	1	0.818	0.091
1	7	0.091	0.636
2	6	0.182	0.545
10	4	0.909	0.364
3	3	0.273	0.273
8	9	0.727	0.818
6	2	0.545	0.182
4	8	0.364	0.727
7	5	0.636	0.455

543 Assume that interest is in values above a threshold u satisfying $P_u = 0.5$, in other words, $P\{Z_2 > u\} =$
 544 $P\{P_2 > P_u\} = 0.5$. In this case we have only one pair, at the index of 7, that satisfy both P_1 and P_2 are
 545 greater than $P_u = 0.5$, thus $P\{Z_1 > u, Z_2 > u\} = P\{P_1 > P_u, P_2 > P_u\} = 1/10 = 0.1$. The calculation
 546 of the empirical tail dependence coefficient is then

547
$$\eta(x_1, x_2) = \frac{\log P\{Z_2 > u\}}{\log P\{Z_1 > u, Z_2 > u\}} = \frac{\log P\{P_2 > P_u\}}{\log P\{P_1 > P_u, P_2 > P_u\}} = \frac{\log(0.5)}{\log(0.1)} = 0.301. \quad (A.1)$$

548

549 **Appendix B Estimate of conditional and joint probabilities of rainfall extremes**

550 The unit Fréchet transformation is given as

$$551 \quad z = \begin{cases} \left(\log \left\{ 1 - \Phi_u \left(1 + \frac{\xi(y-u)}{\sigma_u} \right)^{-1/\xi} \right\} \right)^{-1} & y > u, \xi \neq 0 \\ - \left(\log \left\{ 1 - \Phi_u \exp \left(-\frac{y-u}{\sigma_u} \right)^{-1/\xi} \right\} \right)^{-1} & y > u, \xi = 0 \\ -\{\log F(y_i)\}^{-1} & y \leq u \end{cases} \quad (B.1)$$

552 where y is the original marginal value and z is the Fréchet transformed value and all other parameters
 553 correspond to the GPD specified in Section 4.1. For values below the threshold, F is the empirical
 554 distribution function of y , $F(y_i) = i/(n+1)$ where i is the rank of y_i and n is the total number of data
 555 points.

556 The conditional probability $P\{Z_2 > z_2 | Z_1 > z_1\}$ is obtained from the bivariate inverted max-stable
 557 process cumulative distribution function (CDF) in unit Fréchet margins ([Thibaud et al., 2013](#)), which
 558 is given as:

$$559 \quad P\{Z_1 \leq z_1, Z_2 \leq z_2\} = 1 - \exp\left\{-\frac{1}{g_1}\right\} - \exp\left\{-\frac{1}{g_2}\right\} + \exp[-V\{g_1, g_2\}], \quad (B.2)$$

560 where $g_1 = -1/\log\{1 - \exp(-1/z_1)\}$, $g_2 = -1/\log\{1 - \exp(-1/z_2)\}$, and the exponent measure
 561 V ([Padoan et al., 2010](#)) is defined as:

$$562 \quad V\{g_1, g_2\} = -\frac{1}{g_1} \Phi\left\{\frac{a}{2} + \frac{1}{a} \log \frac{g_2}{g_1}\right\} - \frac{1}{g_2} \Phi\left\{\frac{a}{2} + \frac{1}{a} \log \frac{g_1}{g_2}\right\}. \quad (B.3)$$

563 In Eq. (B.3), Φ is the standard normal cumulative distribution function, $a = \sqrt{2\gamma_{ad}(h)}$ with $\gamma_{ad}(h)$ is
 564 the variograms that was mentioned in the explanation of Eq. (3).

565 In unit Fréchet margins, the relationship between the return level z and the return period T (in number
 566 of observations) is given as $z = -1/\log(1 - 1/T)$, and the conditional probability for the max-stable
 567 process can then be estimated using:

$$568 \quad P\{Z_2 > z_2 | Z_1 > z_1\} = T_1 \left[\frac{1}{T_1} - \exp\left(-\frac{1}{z_2}\right) + P\{Z_1 \leq z_1, Z_2 \leq z_2\} \right], \quad (B.4)$$

569 where T_1 is the return period (in number of observations for 36 hr rainfall) corresponding to the return
 570 level z_1 . It is also noted that in this paper Z_1 and Z_2 were taken as threshold exceedances, so the return
 571 period T_1 should be in the number of observations, which is equivalent to a $T_1/243$ -year return period
 572 because there are 243 observations for 36 hr rainfall in a year.

573 The probability that there is at least one location that has an extreme event exceeding a given threshold
 574 can be calculated based on the addition rule for the union of probabilities, as:

$$\begin{aligned}
 575 \quad P(Z_1 > z_1 \text{ or } \dots \text{ or } Z_N > z_N) &= \sum_{i=1}^N P(Z_i > z_i) - \sum_{i < j} P(Z_i > z_i, Z_j > z_j) + \dots \\
 576 \quad &+ (-1)^{N-1} P(Z_1 > z_1, \dots, Z_N > z_N), \tag{B.5}
 \end{aligned}$$

577 where N is the number of locations.

578 For the case of dependent variables, the joint probability for only two locations $P\{Z_1 > z_1, Z_2 > z_2\}$
 579 can be easily obtained from the bivariate CDF for inverted max-stable process in Eq. (B.2). However,
 580 for the case of multiple locations (five different locations for this paper), it is difficult to derive the
 581 formula for this probability because there are dependences between extreme events at all locations. So
 582 this probability is empirically calculated from a large number of simulations of the dependent model
 583 (see the description of the simulation procedure for an inverted max-stable process in Section 4.3).

584 For the case that all ~~theof~~ events are independent, the joint probability for independent variables is
 585 broken down as the product of the marginals, and the conditional probability is equivalent to the
 586 marginal probability. When applying Eq. (B.5) for independent variables, the joint probability is
 587 therefore calculated by $P(Z_1 > z_1, \dots, Z_N > z_N) = P(Z_1 > z_1) \dots P(Z_N > z_N)$.

588 **Acknowledgments**

589 The lead author was supported by the Australia Awards Scholarships (AAS) from Australia
 590 Government. A/Prof Westra was supported by Australian Research Council Discovery grant
 591 DP150100411. We thank Mark Babister and Isabelle Testoni of WMA Water for providing the
 592 hydrologic models for the case study; and Leticia Mooney for her editorial help in improving this

593 manuscript. The rainfall data used in this study were provided by the Australian Bureau of Meteorology,
594 and can be obtained from the corresponding author.

595 **References**

- 596 Asadi, P., Davison, A. C., and Engelke, S.: Extremes on river networks, *Ann. Appl. Stat.*, 9, 2023-2050,
597 10.1214/15-AOAS863, 2015.
- 598 Ball, J., Babister, M., Nathan, R., Weeks, W., Weinmann, E., Retallick, M., and Testoni, I.: Australian
599 Rainfall and Runoff: A Guide to Flood Estimation, © Commonwealth of Australia (Geoscience
600 Australia), 2016.
- 601 Bárdossy, A., and Pegram, G. G. S.: Copula based multisite model for daily precipitation simulation,
602 *Hydrol. Earth Syst. Sci.*, 13, 2299-2314, 10.5194/hess-13-2299-2009, 2009.
- 603 Baxevani, A., and Lennartsson, J.: A spatiotemporal precipitation generator based on a censored latent
604 Gaussian field, *Water Resources Research*, 51, 4338-4358, doi:10.1002/2014WR016455, 2015.
- 605 Bennett, B., Lambert, M., Thyer, M., Bates, B. C., and Leonard, M.: Estimating Extreme Spatial
606 Rainfall Intensities, *Journal of Hydrologic Engineering*, 21, 04015074, doi:10.1061/(ASCE)HE.1943-
607 5584.0001316, 2016a.
- 608 Bennett, B., Thyer, M., Leonard, M., Lambert, M., and Bates, B.: A comprehensive and systematic
609 evaluation framework for a parsimonious daily rainfall field model, *Journal of Hydrology*,
610 <https://doi.org/10.1016/j.jhydrol.2016.12.043>, 2016b.
- 611 Bernard, M. M.: Formulas for rainfall intensities of long duration, *Transactions of the American Society*
612 *of Civil Engineers*, 96, 592-606, 1932.
- 613 Blanchet, J., and Creutin, J.-D.: Co-Occurrence of Extreme Daily Rainfall in the French Mediterranean
614 Region, *Water Resources Research*, 53, 9330-9349, 10.1002/2017wr020717, 2017.
- 615 Boughton, W., and Droop, O.: Continuous simulation for design flood estimation—a review,
616 *Environmental Modelling & Software*, 18, 309-318, [https://doi.org/10.1016/S1364-8152\(03\)00004-5](https://doi.org/10.1016/S1364-8152(03)00004-5),
617 2003.
- 618 Boyd, M. J., Rigby, E. H., and VanDrie, R.: WBNM — a computer software package for flood
619 hydrograph studies, *Environmental Software*, 11, 167-172, [https://doi.org/10.1016/S0266-
620 9838\(96\)00042-1](https://doi.org/10.1016/S0266-9838(96)00042-1), 1996.
- 621 Cameron, D. S., Beven, K. J., Tawn, J., Blazkova, S., and Naden, P.: Flood frequency estimation by
622 continuous simulation for a gauged upland catchment (with uncertainty), *Journal of Hydrology*, 219,
623 169-187, [https://doi.org/10.1016/S0022-1694\(99\)00057-8](https://doi.org/10.1016/S0022-1694(99)00057-8), 1999.
- 624 Carreau, J., Neppel, L., Arnaud, P., and Cantet, P.: Extreme Rainfall Analysis at Ungauged Sites in the
625 South of France : Comparison of Three Approaches, *Journal de la Société Française de Statistique*, 154
626 No. 2, 119-138, 2013.
- 627 Chow, V. T., Maidment, D. R., and Mays, L. W.: *Applied Hydrology*, McGraw-Hill, c1988, New York,
628 1988.
- 629 Coles, S., Heffernan, J., and Tawn, J.: Dependence Measures for Extreme Value Analyses, *Extremes*,
630 2, 339-365, 10.1023/a:1009963131610, 1999.
- 631 Coles, S.: *An Introduction to Statistical Modeling of Extreme Values*, Springer Series in Statistics,
632 Springer, 2001.
- 633 Davison, A. C., and Smith, R. L.: Models for exceedances over high thresholds, *Journal of the Royal*
634 *Statistical Society. Series B (Methodological)*, 393-442, 1990.
- 635 de Haan, L.: A Spectral Representation for Max-stable Processes, *The Annals of Probability*, 12, 1194-
636 1204, 10.2307/2243357, 1984.
- 637 Demarta, S., and McNeil, A. J.: The t Copula and Related Copulas, *International Statistical Review /*
638 *Revue Internationale de Statistique*, 73, 111-129, 2005.
- 639 Dombry, C., Engelke, S., and Oesting, M.: Exact simulation of max-stable processes, *Biometrika*, 103,
640 303-317, 2016.
- 641 Durocher, M., Chebana, F., and Ouarda, T. B. M. J.: On the prediction of extreme flood quantiles at
642 ungauged locations with spatial copula, *Journal of Hydrology*, 533, 523-532,
643 <https://doi.org/10.1016/j.jhydrol.2015.12.029>, 2016.

644 Favre, A. C., Adlouni, S. E., Perreault, L., Thiémonge, N., and Bobée, B.: Multivariate hydrological
645 frequency analysis using copulas, *Water Resources Research*, 40, doi:10.1029/2003WR002456, 2004.
646 Gupta, A. S., and Tarboton, D. G.: A tool for downscaling weather data from large-grid reanalysis
647 products to finer spatial scales for distributed hydrological applications, *Environmental Modelling &*
648 *Software*, 84, 50-69, <https://doi.org/10.1016/j.envsoft.2016.06.014>, 2016.
649 He, Y., Bárdossy, A., and Zehe, E.: A review of regionalisation for continuous streamflow simulation,
650 *Hydrology and Earth System Sciences*, 15, 3539, 2011.
651 Hegnauer, M., Beersma, J., Van den Boogaard, H., Buishand, T., and Passchier, R.: Generator of
652 Rainfall and Discharge Extremes (GRADE) for the Rhine and Meuse basins; Final report of GRADE
653 2.0, Document extern project, 2014.
654 Hosking, J. R. M., and Wallis, J. R.: *Regional Frequency Analysis - An Approach Based on L-Moments*,
655 Cambridge University Press, Cambridge, UK, 1997.
656 Huser, R., and Davison, A. C.: Composite likelihood estimation for the Brown–Resnick process,
657 *Biometrika*, 100, 511-518, 10.1093/biomet/ass089, 2013.
658 Hüsler, J., and Reiss, R.-D.: Maxima of normal random vectors: Between independence and complete
659 dependence, *Statistics & Probability Letters*, 7, 283-286, [https://doi.org/10.1016/0167-7152\(89\)90106-](https://doi.org/10.1016/0167-7152(89)90106-5)
660 [5](https://doi.org/10.1016/0167-7152(89)90106-5), 1989.
661 Kabluchko, Z., Schlather, M., and de Haan, L.: Stationary Max-Stable Fields Associated to Negative
662 Definite Functions, *The Annals of Probability*, 37, 2042-2065, 2009.
663 Kao, S.-C., and Govindaraju, R. S.: Trivariate statistical analysis of extreme rainfall events via the
664 Plackett family of copulas, *Water Resources Research*, 44, doi:10.1029/2007WR006261, 2008.
665 Kleiber, W., Katz, R. W., and Rajagopalan, B.: Daily spatiotemporal precipitation simulation using
666 latent and transformed Gaussian processes, *Water Resources Research*, 48,
667 doi:10.1029/2011WR011105, 2012.
668 Koutsoyiannis, D., Kozonis, D., and Manetas, A.: A mathematical framework for studying rainfall
669 intensity-duration-frequency relationships, *Journal of Hydrology*, 206, 118-135,
670 [http://dx.doi.org/10.1016/S0022-1694\(98\)00097-3](http://dx.doi.org/10.1016/S0022-1694(98)00097-3), 1998.
671 Kuichling, E.: The relation between the rainfall and the discharge of sewers in populous districts,
672 *Transactions of the American Society of Civil Engineers*, 20, 1-56, 1889.
673 Laurenson, E. M., and Mein, R. G.: RORB Version 4 Runoff Routing Program User Manual, Monash
674 University Department of Civil Engineering, 1997.
675 Le, P. D., Davison, A. C., Engelke, S., Leonard, M., and Westra, S.: Dependence properties of spatial
676 rainfall extremes and areal reduction factors, *Journal of Hydrology*, 565, 711-719,
677 <https://doi.org/10.1016/j.jhydrol.2018.08.061>, 2018a.
678 Le, P. D., Leonard, M., and Westra, S.: Modeling Spatial Dependence of Rainfall Extremes Across
679 Multiple Durations, *Water Resources Research*, 54, 2233-2248, doi:10.1002/2017WR022231, 2018b.
680 Ledford, A. W., and Tawn, J. A.: Statistics for Near Independence in Multivariate Extreme Values,
681 *Biometrika*, 83, 169-187, 1996.
682 Leonard, M., Lambert, M. F., Metcalfe, A. V., and Cowpertwait, P. S. P.: A space-time Neyman–Scott
683 rainfall model with defined storm extent, *Water Resources Research*, 44, doi:10.1029/2007WR006110,
684 2008.
685 Leonard, M., Westra, S., Phatak, A., Lambert, M., Hurk, B. v. d., McInnes, K., Risbey, J., Schuster, S.,
686 Jakob, D., and Stafford-Smith, M.: A compound event framework for understanding extreme impacts,
687 *Wiley Interdisciplinary Reviews: Climate Change*, 5, 113-128, doi:10.1002/wcc.252, 2014.
688 Mulvaney, T. J.: On the use of self-registering rain and flood gauges in making observation of the
689 relation of rainfall and floods discharges in a given catchment, *Proc. Civ. Eng. Ireland*, 4, 18–31, 1851.
690 Nicolet, G., Eckert, N., Morin, S., and Blanchet, J.: A multi-criteria leave-two-out cross-validation
691 procedure for max-stable process selection, *Spatial Statistics*, 22, 107-128,
692 <https://doi.org/10.1016/j.spasta.2017.09.004>, 2017.
693 Oesting, M., Schlather, M., and Friederichs, P.: Statistical post-processing of forecasts for extremes
694 using bivariate Brown–Resnick processes with an application to wind gusts, *Extremes*, 20, 309-332,
695 10.1007/s10687-016-0277-x, 2017.
696 Padoan, S. A., Ribatet, M., and Sisson, S. A.: Likelihood-Based Inference for Max-Stable Processes,
697 *Journal of the American Statistical Association*, 105, 263-277, 10.1198/jasa.2009.tm08577, 2010.

698 Pathiraja, S., Westra, S., and Sharma, A.: Why continuous simulation? The role of antecedent moisture
699 in design flood estimation, *Water Resources Research*, 48, doi:10.1029/2011WR010997, 2012.

700 Pickands, J.: Statistical Inference Using Extreme Order Statistics, *The Annals of Statistics*, 3, 119-131,
701 10.2307/2958083, 1975.

702 Rahman, A., Weinmann, P. E., Hoang, T. M. T., and Laurenson, E. M.: Monte Carlo simulation of flood
703 frequency curves from rainfall, *Journal of Hydrology*, 256, 196-210, [https://doi.org/10.1016/S0022-1694\(01\)00533-9](https://doi.org/10.1016/S0022-1694(01)00533-9), 2002.

704 Rasmussen, P. F.: Multisite precipitation generation using a latent autoregressive model, *Water
705 Resources Research*, 49, 1845-1857, doi:10.1002/wrcr.20164, 2013.

706 Renard, B., and Lang, M.: Use of a Gaussian copula for multivariate extreme value analysis: Some case
707 studies in hydrology, *Advances in Water Resources*, 30, 897-912,
708 <http://dx.doi.org/10.1016/j.advwatres.2006.08.001>, 2007.

709 Requena, A. I., Chebana, F., and Ouarda, T. B. M. J.: A functional framework for flow-duration-curve
710 and daily streamflow estimation at ungauged sites, *Advances in Water Resources*, 113, 328-340,
711 <https://doi.org/10.1016/j.advwatres.2018.01.019>, 2018.

712 Russell, B. T., Cooley, D. S., Porter, W. C., and Heald, C. L.: Modeling the spatial behavior of the
713 meteorological drivers' effects on extreme ozone, *Environmetrics*, 27, 334-344, doi:10.1002/env.2406,
714 2016.

715 Schlather, M.: Models for Stationary Max-Stable Random Fields, *Extremes*, 5, 33-44,
716 10.1023/A:1020977924878, 2002.

717 Seneviratne, S. I., Nicholls, N., Easterling, D., Goodess, C. M., Kanae, S., Kossin, J., Luo, Y., Marengo,
718 J., McInnes, K., and Rahimi, M.: Managing the Risks of Extreme Events and Disasters to Advance
719 Climate Change Adaptation: Changes in Climate Extremes and their Impacts on the Natural Physical
720 Environment, 2012.

721 Nambucca Heads Flood Study:
722 http://www.nambucca.nsw.gov.au/cp_content/resources/16152_2011_Nambucca_Heads_Flood_Study_Final_Draft_Chapter_6a.pdf, 2011.

723 Stedinger, J., Vogel, R., and Foufoula-Georgiou, E.: Frequency Analysis of Extreme Events, in:
724 Handbook of Hydrology, edited by: Maidment, D. R., McGraw-Hill, New York, 18.11-18.66, 1993.

725 Stephenson, A. G., Lehmann, E. A., and Phatak, A.: A max-stable process model for rainfall extremes
726 at different accumulation durations, *Weather and Climate Extremes*, 13, 44-53,
727 <https://doi.org/10.1016/j.wace.2016.07.002>, 2016.

728 Thibaud, E., Mutzner, R., and Davison, A. C.: Threshold modeling of extreme spatial rainfall, *Water
729 Resources Research*, 49, 4633-4644, 10.1002/wrcr.20329, 2013.

730 Wadsworth, J. L., and Tawn, J. A.: Dependence modelling for spatial extremes, *Biometrika*, 99, 253-
731 272, 10.1093/biomet/asr080, 2012.

732 Wang, Q. J.: A Bayesian Joint Probability Approach for flood record augmentation, *Water Resources
733 Research*, 37, 1707-1712, 10.1029/2000WR900401, 2001.

734 Wang, Q. J., Robertson, D. E., and Chiew, F. H. S.: A Bayesian joint probability modeling approach
735 for seasonal forecasting of streamflows at multiple sites, *Water Resources Research*, 45,
736 doi:10.1029/2008WR007355, 2009.

737 Wang, X., Gebremichael, M., and Yan, J.: Weighted likelihood copula modeling of extreme rainfall
738 events in Connecticut, *Journal of Hydrology*, 390, 108-115,
739 <http://dx.doi.org/10.1016/j.jhydrol.2010.06.039>, 2010.

740 Westra, S., and Sisson, S. A.: Detection of non-stationarity in precipitation extremes using a max-stable
741 process model, *Journal of Hydrology*, 406, 119-128, <http://dx.doi.org/10.1016/j.jhydrol.2011.06.014>,
742 2011.

743 WMAWater: Review of Bellinger, Kalang and Nambucca River Catchments Hydrology, Bellingen
744 Shire Council, Nambucca Shire Council, New South Wales Government, 2011.

745 Zhang, L., and Singh, V. P.: Gumbel's Hougaard Copula for Trivariate Rainfall Frequency
746 Analysis, *Journal of Hydrologic Engineering*, 12, 409-419, doi:10.1061/(ASCE)1084-
747 0699(2007)12:4(409), 2007.

748 Zheng, F., Westra, S., and Leonard, M.: Opposing local precipitation extremes, *Nature Clim. Change*,
749 5, 389-390, 10.1038/nclimate2579

752 <http://www.nature.com/nclimate/journal/v5/n5/abs/nclimate2579.html#supplementary-information>,
753 2015.
754 Zscheischler, J., Westra, S., van den Hurk, B. J. J. M., Seneviratne, S. I., Ward, P. J., Pitman, A.,
755 AghaKouchak, A., Bresch, D. N., Leonard, M., Wahl, T., and Zhang, X.: Future climate risk from
756 compound events, Nature Climate Change, 8, 469-477, 10.1038/s41558-018-0156-3, 2018.

757